Mixed experimental/numerical methods applied for concrete parameters estimation

T. Gajewski & T. Garbowski
Poznan University of Technology, Poland
Institute of Structural Engineering
ul. Piotrowo 5, 60-965 Poznan

ABSTRACT: Mixed numerical/experimental method is one of the most widely used for solving difficult practical inverse problems of great industrial significance. Here the mechanical characterization of concrete as one of the most popular construction material is presented. Through a typical uniaxial test of cubic concrete specimen enhanced by in-plane contactless displacement measurements the full set of material constants in typical elasto-plastic constitutive models can be estimated. The great benefit of proposed identification technique is reduction in number of required experimental efforts to just a single test. Such approach provides economical and robust inverse procedure which can be easily conducted in typical testing laboratory.

1 INTRODUCTION

Estimation of the material parameters belongs to the category of parameter identification and is very important from the point of view of industrial applications. Moreover, for newly designed structures which intend to work in plastic region, all the experiments involved in the estimation procedure must take into account also the identification of inelastic parameters.

There are few works reported in the literature that deal with the estimation of material properties through judicious use of the experimentally obtained structural response and the response of the mathematical model of the structure (see e.g. Zirpoli et al. 2008, Bolzon and Buljak 2011, Garbowski et al. 2011). These methods belong to the more general class of solution techniques called Mixed Numerical/Experimental Technique (MNET). Methods belonging to this class differ among themselves in the data that are chosen for comparison and in the method of updating the design variables. For example in Garbowski et al. (2012) authors dealt with the in-plane field of deformations generated by nonstandard biaxial test of the cruciform-shaped thin foil sample, where the error functional was the sum of the squared differences of measured and computed displacements. The set of interesting examples on synergic combinations of computational methods and experiments for structural diagnoses can be found in Maier et al. (2010) or in Maier et al. (2014). However, all of them used the same numerical technique, i.e., nonlinear optimization with constraints, which falls in the category of classical optimization.

The classical form of minimization problem with box constraints reads:

$$\arg\min_{\mathbf{x}} \left\{ \left[\mathbf{U}_E - \mathbf{U}_N(\mathbf{x})\right]^T \mathbf{C}^{-1} \left[\mathbf{U}_E - \mathbf{U}_N(\mathbf{x})\right] \right\}, \quad (1)$$

$$\mathbf{lb} \leq \mathbf{x} \leq \mathbf{ub}$$

where $\mathbf{x}$ is a vector of sought parameters, $\mathbf{U}_E$ is a vector of measurable quantities, $\mathbf{U}_N$ is a vector of computed responses, $\mathbf{C}$ is a covariance matrix, $\mathbf{lb}$ is a vector of lower bounds of parameters and $\mathbf{ub}$ is a vector of upper bounds of parameters.

The minimization of nonlinear objective function subjected to constraints is a challenging task especially when the function appears to be also nonconvex (multimodal). The first-order minimization algorithms usually employed at first attempt belong to the gradient based class of deterministic optimization method. Among them scaled conjugate gradient, Gauss-Newton or Levenberg-Marquardt algorithm developed in Trust Region or Line Search framework are the most frequently used (see e.g. Nocedal & Wright 2006). The main difference between trust region and line search approach is how the step length and its direction is computed in the new iteration. One of the main issues of the trust region approach, which to a large extent determines the success and the performance of this algorithm, is in deciding how large the trusted region should be. Allowing it to

be too large can cause the algorithm to face the same problem as the classical Newton direction line search, when the model function minimizer is quite distinct from the minimizer of the actual objective function. On the other hand using too small region means that the algorithm will miss the opportunity to take a step substantial enough to move it much closer to the solution. In contrary using the line search approach the step length in each iteration has to be adjusted with a cost of additional function calls, i.e. direct model evaluation.

The common feature of discussed algorithms (provided they are implemented in the least square framework) is that there is no need to construct a Hessian (matrix of second order partial derivatives of objective function with respect to model parameters) because it is computed 'for free' from Jacobian:

$$\mathbf{H}(\mathbf{x}) \simeq \mathbf{J}^T\mathbf{J}, \tag{2}$$

where Jacobian ($\mathbf{J}$) is a first order partial derivative of residual vector ($\mathbf{R} = \mathbf{U}_E - \mathbf{U}_N(\mathbf{x})$) with respect to vector of parameters $\mathbf{x}$, namely:

$$\mathbf{J} = \frac{\partial \mathbf{R}}{\partial \mathbf{x}}. \tag{3}$$

This approximation, however, is valid only if the residuals are small, meaning we are close to the solution. Therefore some techniques may be required in order to ensure that the Hessian matrix is semi-positive defined, see e.g. (Nocedal & Wright 2006). Regardless of whether Trust Region or Line Search framework for gradient-based algorithms is used the main drawback is that they remain local, meaning the solution strongly depends on starting point.

Another important class of methods frequently employed for the minimization of nonconvex functions are global optimization techniques, e.g. Genetic or Evolutionary Algorithms (Dlugosz and Burczynski 2012), Particle Swarm Algorithm (Burczynski and Szczepanik 2013) or Simulated Annealing (Wierzchon et al. 2010), which do not require the gradient computations. Without information about gradient another method of choosing the direction and step length of new iteration had to be selected. For example Genetic Algorithms use an evolution theory, keeping most suited individuals for next generation, and cross-overing or mutating remaining individuals in population. Particle Swarm Algorithm iteratively improves a candidate position by moving all particles around in the search-space according to simple mathematical formula over the particle's position and velocity. Each particle's movement is influenced by its local best known position and is also guided toward the best known positions in the search-space, which are updated when better positions are found by other particles. This is expected to move the swarm toward the best solutions. The main drawback of these methods is that they require hundreds or even thousands of iterations (direct model computation) which make them hardly applicable in solving the practical engineering problems.

The technique adopted here for estimating the material properties combines a standard uniaxial compression test of cubic concrete specimen, noncontacting method of displacement field measurements and nonlinear least square approach for discrepancy function minimization. In the following section the main ideas of proposed method will be briefly described, details concerning inverse procedure and experimental set up are presented in the previous work of Gajewski & Garbowski (2014).

The main aim of this work is to extend the applicability of our previously proposed identification methodology to a wider family of constitutive models of concrete. Here, the Drucker-Prager model with its various modifications, commonly used in many practical applications, is successfully calibrated.

2 EXPERIMENTAL SET-UP

2.1 *Enhanced compression test*

From practical point of view the identification of material parameters should be a procedure which is reasonable simple to conduct. Due to this fact, in this research standard uniaxial compression test of concrete is considered, as an experiment which can be performed in any civil engineering laboratory with typical experimental set-up on uniaxial testing machine.

First of all, cubic specimen should be prepared with normalized procedures, i.e. proper curing of concrete, sufficient time of strengthening, recommended dimensions: $0.15 \times 0.15 \times 0.15$ [m^3]. Upper and lower specimen faces should be slightly polished to improve surface smoothness.

Furthermore material examination should be performed under standard conditions, typically specimen is compressed between two rigid plates, with application of quasi-static displacement/load to the upper surface of specimen during test. Boundary conditions velocity should be $0.2 - 1.0$ MPa/s with strain rate not exceeding 10^{-6} 1/s. In presented paper experiments was carried out on an Instron 8500 (www.instron.tm.fr) four-column frame servo-hydraulic fatigue testing machine with compressive force capacities of up to 1000 kN (see Fig. 1) with displacement protocol.

Through traditional test just few concrete parameters can be recognized, such as the Young modulus E, the compressive strength σ_c or the crushing energy G. In this research we challenge to identify several more variables embedded in a class of Drucker-Prager constitutive laws (detailed description will be presented in forthcoming section) without arranging additional experiments on material sample. Therefore introduced typical compression test should be

Figure 1: Hydraulic testing machine Instron 8500 for performing static, fatigue and dynamic tests

enhanced by additional procedure, which will extract more information from a single test.

For this purpose, noncontacting measurements of displacements field by digital image correlation (DIC) is considered to be performed. Main idea of combining DIC with compression test is to obtain displacements field on the specimen front surface by camera images in certain snapshots of applied upper surface displacement. In addition to enriched experimental data, numerical model of phenomena should be build, where the only unknowns will be material parameters. Hence by solving inverse problem, namely minimizing discrepancy between two measurements (experimentally measured and numerically computed displacements on each iteration) material parameters of applied constitutive law can be determined.

2.2 *Digital image correlation*

Digital image correlation employment in experimental tests can significantly improve material characterization. Nowadays such measurement technique is widely developed and used for practical engineering problems, (see e.g. Garbowski et al. 2011, Bolzon et al. 2012, Tekieli and Slonski 2013). The general idea is to obtain displacements or strains field only by analyzing pictures of recorded object, in our case displacements of front specimen surface are tracked.

DIC system requires the following elements: specially prepared surface of sample (white-black randomly sprayed a paint pattern called speckle pattern), digital camera (for taking pictures during measurements) and correlation software (here home-made code was developed).

Correlation algorithm uses data stored in monochromatic pictures, namely color values of pixels, which vary between 0 and 255, which correspond to black and white color, respectively. Region of image interest is divided into small zones of interest (ZOI), which later forms vertex of displacement field mesh. Function in eq. (4) measures how well

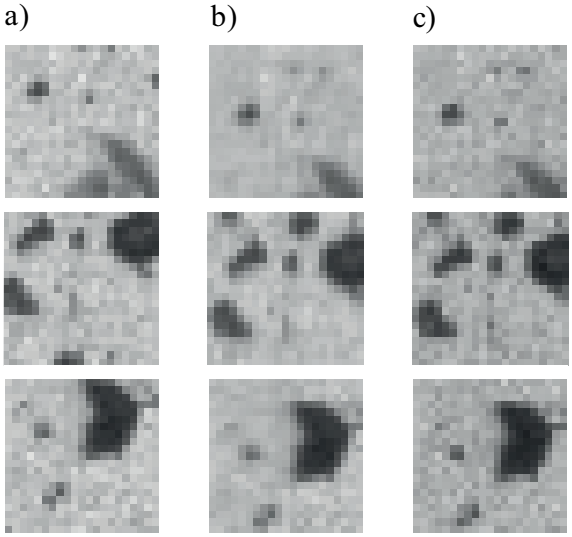

Figure 2: Different three ZOI examples of DIC determination, column (a) reference images from camera, column (b) converged (computed) solutions and column (c) deformed images - original from camera

data from two images (on ZOI level), namely: (i) an experimental field of displacements - $f(x,y)$ (with particular displacement/load applied) and (ii) $g(x',y')$ - a computed field of displacements (on the basis of undeformed state picture), correlates.

$$S\left(x,y,u,v,\frac{\partial u}{\partial x},\frac{\partial u}{\partial y},\frac{\partial v}{\partial x},\frac{\partial v}{\partial y}\right) = \\ = 1 - C_i(f\,(x,y)\,,g\,(x',y')). \tag{4}$$

Computed solution is iteratively improved by minimization algorithm, which searches for a desired values of deformation field of ZOI (displacements x and y, normal strains u and v and finally shape changes $\partial u/\partial x$, $\partial u/\partial y$, $\partial v/\partial x$ and $\partial v/\partial y$). In a criterion C_i different types of formulas can be used, the most robust are zero normalized cross-criterion (ZNCC) and zero normalized sum squared difference (ZNSSD), their advantage among others criterion is e.g. insensitivity to variations in lighting conditions, (for more details see e.g. Pan et al. 2009, Sutton et al. 2009).

Finally the robust optimization algorithm should be used. In this research Newton-Raphson method was involved, where the procedure focus on calculation of correction terms which are changed in each iteration starting from initial guess. Hence the starting point needs to be relatively close to optimal solution.

Three ZOI examples of DIC home-made software exploration are presented in the Fig. 2, where middle column shows converged solutions (which is calculated in optimization loop only by modifying fields from left hand side column - undeformed state) to images taken during test (right hand side). For each case (row) unknown values of x, y, u, v, $\partial u/\partial x$, $\partial u/\partial y$, $\partial v/\partial x$ and $\partial v/\partial y$ were obtained.

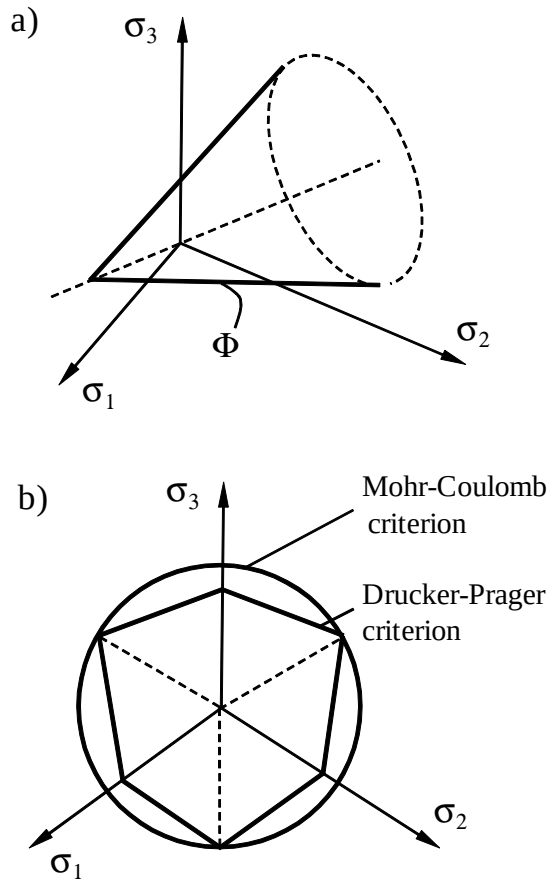

Figure 3: (a) Yield surface according to the DP criterion in principal stress space, (b) Deviatoric plane of DP and Mohr-Coulomb criterion in terms of principal stress

3 DRUCKER-PRAGER PLASTICITY

3.1 *Introduction*

Depending on the purpose of representing specific state of material (e.g. complex stress state, plastic behavior or creep) various models of concrete can be employed. Concrete as a composite and granular material needs peculiar description of constitutive behavior. Many concrete models can be found in the literature, e.g. Rankine 1857, Resende and Martin 1985, Lubliner et al. 1989. Among them one of the most known and commonly used for granular material is Drucker-Prager model originally proposed to describe soil behavior by Drucker & Prager (1952) with later modifications and extensions.

Drucker-Prager (DP) model is pressure-dependent yield criterion (see Fig. 3a) where the plastic yielding occurs when following equation is satisfied:

$$\sqrt{J_2(\mathbf{s})} + \eta p = d, \tag{5}$$

where p is the equivalent pressure stress, J_2 the second invariant of the deviatoric stress and η and d are material constants. It is worth to underline that discussed constitutive law is a smooth approximation of the Mohr-Coulomb (MC) yield criterion. Material model is formulated in terms of principal stress σ_i or stress invariants and is represented geometrically by circular cone with axis on the hydrostatic line. In addition, von Mises yield shape can be reconstructed if $\eta = 0$.

Before further description would be recalled several definitions have to be introduced, namely equivalent pressure stress p, Mises equivalent stress q and third invariant of deviatoric stress r, determined respectively, as:

$$\begin{aligned} p &= -\frac{1}{3} tr\left(\boldsymbol{\sigma}\right), \\ q &= \sqrt{\frac{3}{2}\left(\mathbf{s} : \mathbf{s}\right)}, \\ r &= \left(\frac{9}{2}\mathbf{s}\cdot\mathbf{s} : \mathbf{s}\right)^{1/3} \end{aligned} \tag{6}$$

where **s**, deviatoric stress, is calculated by the formula $\mathbf{s} = \boldsymbol{\sigma} + p\mathbf{I}$, with **I** as the second order identity tensor.

As previously indicated Drucker-Prager yield criterion can approximate Mohr-Coulomb surface shape (see Fig. 3b), after reference (de Souza Neto et al. 2008) yield function takes the form:

$$\Phi(\boldsymbol{\sigma}, d) = \sqrt{J_2\left(\mathbf{s}\left(\boldsymbol{\sigma}\right)\right)} + \eta p\left(\boldsymbol{\sigma}\right) - \xi d, \tag{7}$$

where η and ξ are selected from Mohr-Coulomb law. Moreover yield surface of DP surface can coincident with Mohr-Coulomb in two particular cases, on the outer and inner edges of MC surface. For outer position η and ξ should be read as:

$$\eta = \frac{6\sin\beta}{\sqrt{3}\left(3 - \sin\beta\right)}, \qquad \xi = \frac{6\cos\beta}{\sqrt{3}\left(3 - sin\beta\right)}, \tag{8}$$

and for outer locus:

$$\eta = \frac{6\sin\beta}{\sqrt{3}\left(3 + \sin\beta\right)}, \qquad \xi = \frac{6\cos\beta}{\sqrt{3}\left(3 + \sin\beta\right)}, \tag{9}$$

where β is the angle of internal friction (opening angle of yield surface cone in principal stress space, known from Mohr-Coulomb law). Received cones are called *compression* and *extension* cone, respectively, for further details see (de Souza Neto et al. 2008).

3.2 *Yield surface functions*

Drucker-Prager models can vary between different geometrical description of yield surface, from the simplest - linear, through hyperbolic, to the most general one - exponential relation.

Linear representation. Usually yield surface of material is described by linear law:

$$\Phi\left(\boldsymbol{\sigma}, d\right) = t - p\tan\beta - d = 0, \tag{10}$$

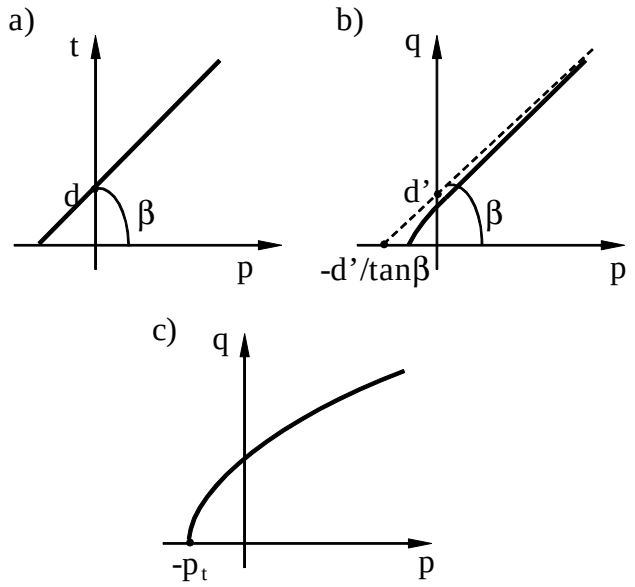

Figure 4: Different geometrical representation of DP yield criterion in meridional plane: (a) linear, (b) hyperbolic, (c) exponential

where d is the cohesion pressure of the material and t, deviatoric stress measure, is defined by:

$$t = \frac{1}{2}q\left[1 + \frac{1}{K} - \left(1 - \frac{1}{K}\right)\left(\frac{r}{q}\right)^3\right],$$

where K, called flow ratio, is the ratio between the yield stress in triaxial tension and the yield stress in triaxial compression. Influence of flow ratio K can be simply presented in the deviatoric plane, which is calculated in the terms of principal stresses σ_i, see Fig. 3b. The yield surface convexity is ensured when following condition is satisfied $0.778 \leq K \leq 1$. Finally, when K is equal 1.0, t reduces to q.

In linear description, the projection of principal stress in $p - t$ plane called meridional plane is introduced. The example of typical linear yield surface in meridional plane is presented on the Fig. 4a.

Hyperbolic form. For this extension of the DP model (see Fig. 4b), yield function reads:

$$\Phi = \sqrt{\left(\bar{d}^0 - p_t^0 tan\beta\right)^2 + q^2} - p\tan\beta - \bar{d} = 0, \quad (11)$$

with $\bar{d}^0$ – initial cohesion of the material, p_t^0 – initial hydrostatic tension strength of the material and β – frictional angle measured for high pressure values. Presented eq. (11) is a mixed formulation of maximum tensile stress (for lower and negative values of pressures) and linear DP criterion (for high pressures).

Exponent relation. The most general yield surface representation (see Fig. 4c) can be defined by exponential function:

$$\Phi = aq^b - p - p_t = 0, \quad (12)$$

where a and b are the constants of function in p-q plane and p_t is the hydrostatic tension strength of the material.

3.3 *Plastic flow*

In multidimensional plasticity models the existence of flow potential is assumed:

$$\Psi = \Psi\left(\boldsymbol{\sigma}, \kappa\right), \quad (13)$$

where κ is hardening thermodynamical force. Two class of flow rule, called *associative* and *non-associative* potential, can be distinguished. *Associative* models read:

$$\Psi \equiv \Phi, \quad (14)$$

where plastic potential Ψ is equal to yield function. In such models evolution of plastic surface is calculated by expression

$$\dot{\varepsilon}^p = \dot{\gamma}\frac{\partial\Psi}{\partial\sigma}, \quad (15)$$

where $\dot{\gamma}$ is the plastic multiplier. In addition plastic strain rate is normal to the yield surface (unlike in the *non-associative* rule). Although if flow potential Ψ is different then yield function Φ then *non-associative* description is considered, for further details see e.g. de Souza Neto et al. 2008.

4 PSEUDO-EXPERIMENTAL EXAMPLES

In mixed numerical/experimental techniques pseudo-experimental verification play crucial role before conducting inverse procedure examination on real test data. In the first place we have to assume values of sought parameters (inputs), which later will be searched and called *reference* one. Moreover, two different FE models should be prepared, one to obtain pseudo-experimental quantities (outputs) for assumed reference parameters (e.g. system with finer mesh) and second for inverse analysis performance. Recent model will be submitted on each step of procedure to minimize the differences in displacements between pseudo-experimental field (noised and truncated to the accuracy of 1μm, two orders less then applied displacement) and numerical one.

Here the compression test was modeled by one quarter of cubic specimen with relevant symmetrical conditions and application of upper surface vertical displacement of few millimeters. Sample space was discretized by 4960 number of solid three-dimensional eight-node reduced integration elements with linear shape functions.

Results of concrete characterization through pseudo-experimental data are depicted in Figs. 6-14. Each plot shows the calibration procedure of different

Table 1: The residual discrepancy of identified parameter with respect to their reference values represented in percentage

DP surface	hardening def.	E	β	K	ψ	σ_0	H	p_t^0	a	b
linear	compression	0.1	1.5	0.3	0.3	0.1	1.9	–	–	–
	shear	0.3	0.3	0.2	0.0	0.2	1.0	–	–	–
	tension	0.0	2.7	1.1	0.5	0.1	2.1	–	–	–
hyperbolic	compression	0.2	0.3	–	0.4	0.1	0.8	0.5	–	–
	shear	0.2	0.7	–	1.0	0.6	1.4	2.4	–	–
	tension	0.0	1.0	–	1.1	0.6	1.7	1.5	–	–
exponential	compression	0.5	–	–	0.1	0.2	1.6	–	16.2	1.4
	shear	0.0	–	–	0.0	0.0	0.0	–	11.2	0.7
	tension	0.2	–	–	0.1	0.1	0.4	–	45.6	1.7

form of yield criteria Φ in Drucker-Prager constitutive function, namely linear (Figs. 6-8), hyperbolic (Figs. 9-11) and exponential (Figs. 12-14). Yield surface groups can be classified further, due to its hardening definition. For each type of DP law, evolution of the yield surface described in terms of the equivalent stress may be defined in yield stress of uniaxial compression (Figs. 6, 9, 12), shear (cohesion, Figs. 7, 10, 13) or uniaxial tension (Figs. 8, 11, 14).

Figures 6-14 in (a) subplots illustrate convergence of the inverse analysis to the normalized values of parameters (x_i/x_i^{REF}), (b) subplots demonstrate the progressive changes of objective function. At this point it is important to underline that the characteristic plateaus, observed on objective function plots (see Figs. 6b-14b), are due to noisy pseudo-experimental data used in all examples.

According to the presented results in most cases unknown parameters converge to their reference values (i.e. to one in the normalized space) after $6-16$ iterations, the only exception is hyperbolic DP with hardening defined by tension, where more then 35 iterations were required.

In the Tab. 1 the brief summary of all performed numerical examples is presented. Taking together all parameters embedded in different constitutive variation of DP model, namely: E - the Young modulus, β - the internal angle of friction, K - the ratio of the yield stress in triaxial tension to the yield stress in triaxial compression, Ψ - the dilatation angle, H - the hardening slope, σ_0 - the yield stress, p_t^0 - the initial hydrostatic tension strength and a, b - the linear, exponential coefficient, respectively, all corresponding discrepancies between identified active parameters and their reference values are gathered in the Table.

As it can be noticed, most of the inverse analyses converged to the right solution with a discrepancy on the reasonably low level (usually below 2%). This confirms that the proposed mixed experimental/numerical method applied for DP material model characterization is valid and robust. It is also visible that for some parameters (e.g. a in an exponential variation of DP) the discrepancy is rather high which can be justified by a low sensitivity of measurements with respect to this particular parameter.

The sensitivity analysis was conducted here for each case separately, however, because it is beyond the main scope of this paper only one plot is here presented, see Fig. 5. The example considers exponential DP analysis with compression hardening. This is to demonstrate that the sensitivities of measurable quantities (here the vertical and horizontal displacements and reaction force) with respect to parameter a are significantly smaller then for other constants. Due to low sensitivities of this parameter its identification is unlikely what can be also noticed in Figs. 12-14.

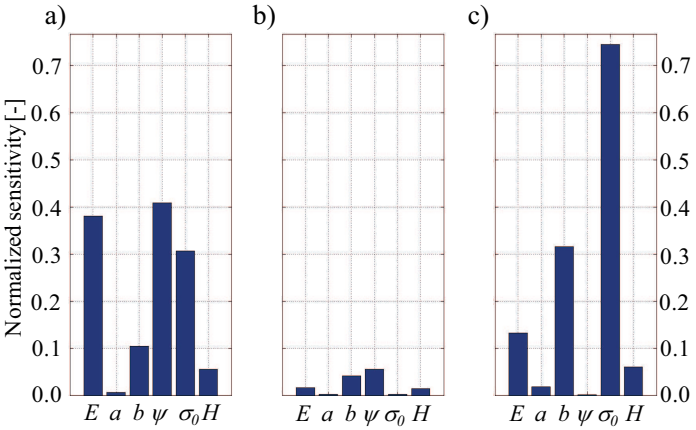

Figure 5: Sensitivities of measurable quantities: (a) displacements field in x-direction, (b) displacements field in y-direction and (c) reaction forces, with respect to the **exponential** DP model parameters with hardening defined by **shear** yield stress

Formal expression for sensitivity calculations are as follows:

$$s_{ux}(x_i) = \sum_{n=1}^{N} \left\{ \frac{1 - \|\mathbf{u}_n^x(x_i)\| \,/\, \|\mathbf{u}_n^x(x_i^{\text{REF}})\|}{\delta} \right\} \tag{16}$$

$$s_{uy}(x_i) = \sum_{n=1}^{N} \left\{ \frac{1 - \|\mathbf{u}_n^y(x_i)\| \,/\, \|\mathbf{u}_n^y(x_i^{\text{REF}})\|}{\delta} \right\} \tag{17}$$

$$s_r(x_i) = \sum_{n=1}^{N} \left\{ \frac{1 - r_n(x_i)/r_n(x_i^{\text{REF}})}{\delta} \right\} \tag{18}$$

where $s_{ux}(x_i)$, $s_{uy}(x_i)$, $s_r(x_i)$ are sensitivity values for i-th parameter in terms of horizontal displacement u_x, vertical displacement u_y and reaction force

of upper concrete surface in vertical direction r, respectively; δ is perturbation value and equals 0.01; $\mathbf{u}_n^x(x_i^{\text{REF}})$, $\mathbf{u}_n^y(x_i^{\text{REF}})$ and $r_n(x_i^{\text{REF}})$ are reference displacement fields (in x and y direction) and reaction, respectively (computed by pseudo-experimental FE model in n-th snapshot); $\mathbf{u}_n^x(x_i)$, $\mathbf{u}_n^y(x_i)$ and $r_n(x_i)$ are fields computed in similar way but by the numerical model in inverse procedure; $n = 1 \dots N$ is a snapshot number (here the total number of intervals N is equal 10).

5 CONCLUSIONS

Calibration of concrete material with its numerous constitutive parameters usually requires several tests at different level of difficulties and specimen configurations. Here, a simple procedure combining a standard uniaxial test, DIC measurements and inverse analysis highlights a successful characterization of the selected material constants for concrete. By a proper selection of identification tools, namely a fast DIC algorithm, a robust minimization technique and a careful selection of the appropriate constitutive model for a numerical test simulation, one can easily find a set of sought parameters from a single and typical laboratory test.

Additional equipment (such as a camera and DIC algorithm) resulting in additional measurements from a single test, clearly helps to identify more parameters. Such an approach, however, also requires a computer with specialized software for both photograph correlation and numerical simulations. This might be viewed as a limitation especially when tests have to be performed on a routine basis in laboratories. A remedy to the underlined limitation of the presented method could be to preliminarily prepare the models and to simulate the tests on a powerful computer, using a wide range of variations in parameters, which can be later used to build an approximation of the model. Using model reduction techniques (such as artificial neural networks, polynomial approximation, radial basis functions approximation, Gaussian processes, etc.), one can speed up parameter identification by several orders of magnitude.

The methodology presented in this paper of identification of concrete parameters from a single test can furthermore be successfully used without heavy computation so long that an approximation of the direct model has been constructed. The numerical model and/or its surrogate require the previously presented combination of DIC measurements together with a rapid correlation algorithm, and efficient experimental and inverse techniques in order to provide a fast and robust characterization of a complex model from a simple test. It is evident from the presented examples that standard testing information (i.e. the force-displacement curve) enhanced with DIC measurement and inverse analysis can be used to successfully calibrate a concrete material model.

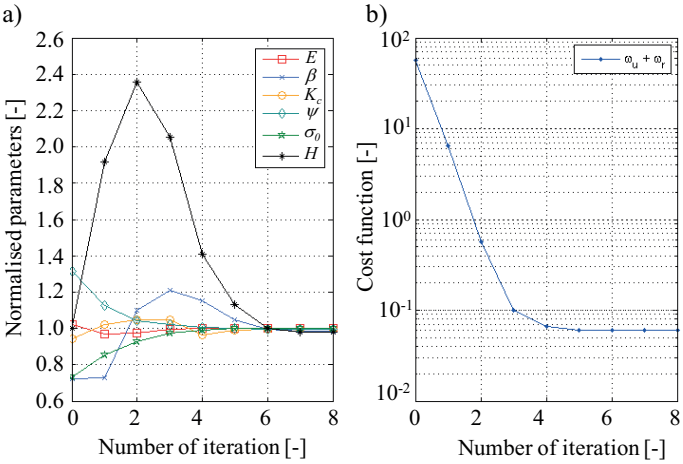

Figure 6: (a) Convergence curves for **linear DP** constitutive law with hardening defined by **compression** yield stress σ_0, pseudo-experimental approach with noised data (accuracy - 1μm), (b) Convergence of cost function

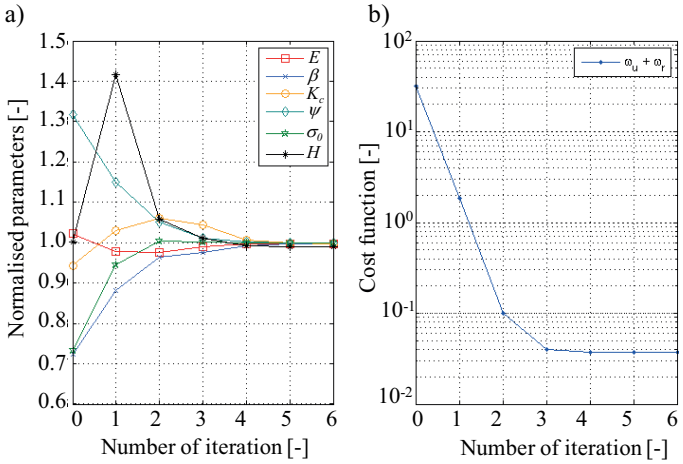

Figure 7: (a) Convergence curves for **linear DP** constitutive law with hardening defined by **shear** yield stress σ_0, pseudo-experimental approach with noised data (accuracy - 1 μm), (b) Convergence of cost function

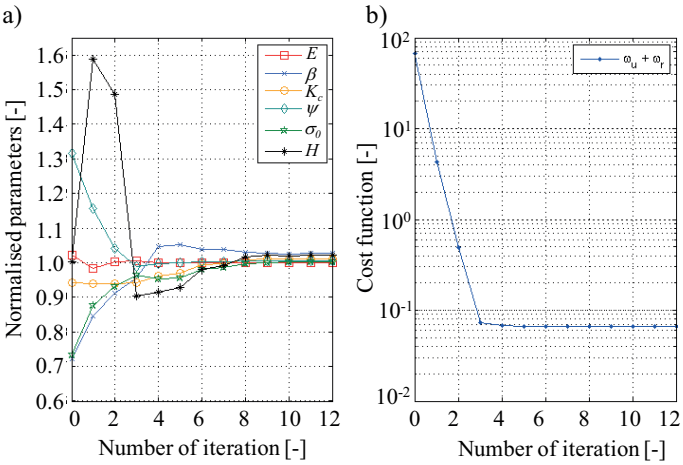

Figure 8: (a) Convergence curves for **linear DP** constitutive law with hardening defined by **tension** yield stress σ_0, pseudo-experimental approach with noised data (accuracy - 1μm), (b) Convergence of cost function

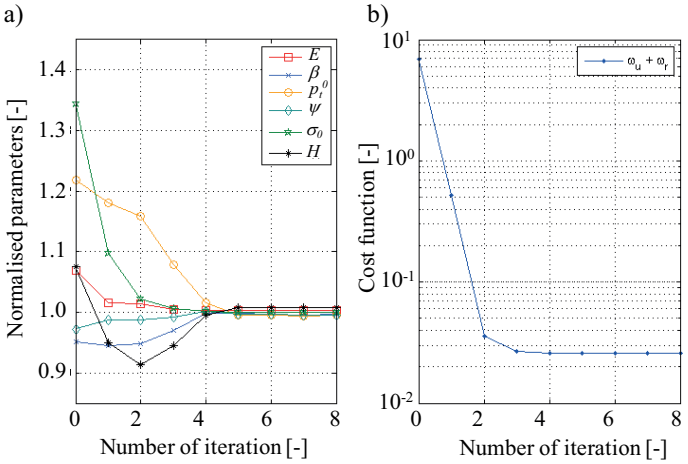

Figure 9: (a) Convergence curves for **hyperbolic DP** constitutive law with hardening defined by **compression** yield stress σ_0, pseudo-experimental approach with noised data (accuracy - 1μm), (b) Convergence of cost function

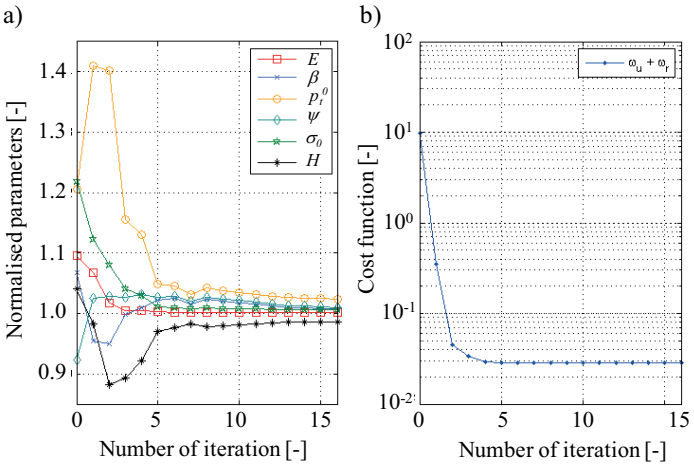

Figure 10: (a) Convergence curves for **hyperbolic DP** constitutive law with hardening defined by **shear** yield stress σ_0, pseudo-experimental approach with noised data (accuracy - 1μm), (b) Convergence of cost function

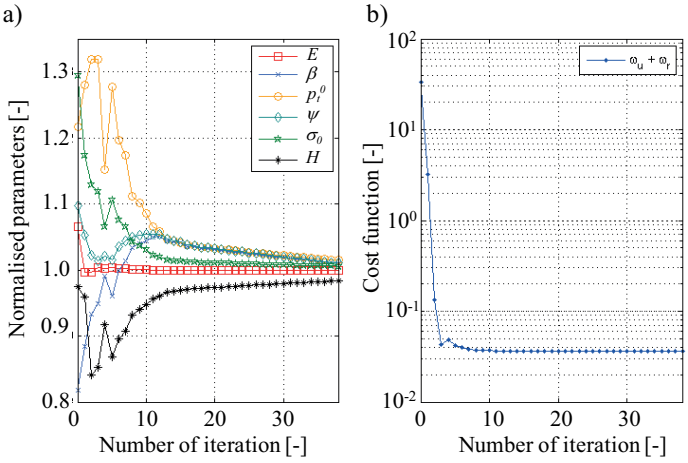

Figure 11: (a) Convergence curves for **hyperbolic DP** constitutive law with hardening defined by **tension** yield stress σ_0, pseudo-experimental approach with noised data (accuracy - 1μm), (b) Convergence of cost function

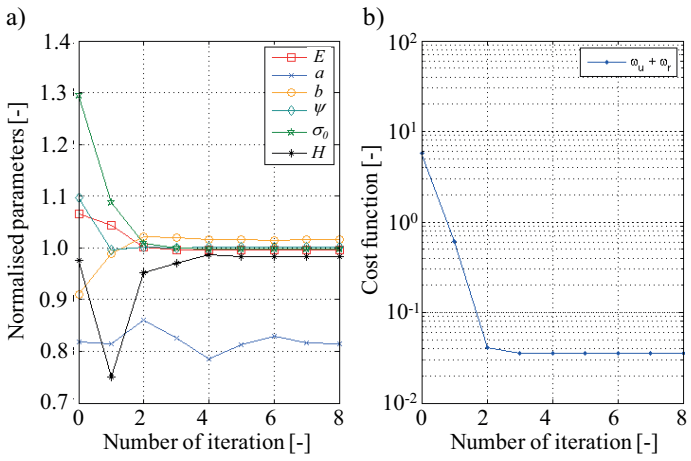

Figure 12: (a) Convergence curves for **exponential DP** constitutive law with hardening defined by **compression** yield stress σ_0, pseudo-experimental approach with noised data (accuracy - 1μm), (b) Convergence of cost function

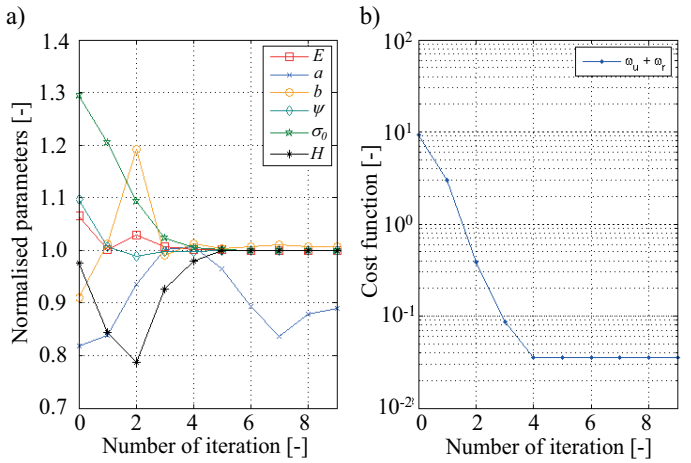

Figure 13: (a) Convergence curves for **exponential DP** constitutive law with hardening defined by **shear** yield stress σ_0, pseudo-experimental approach with noised data (accuracy - 1μm), (b) Convergence of cost function

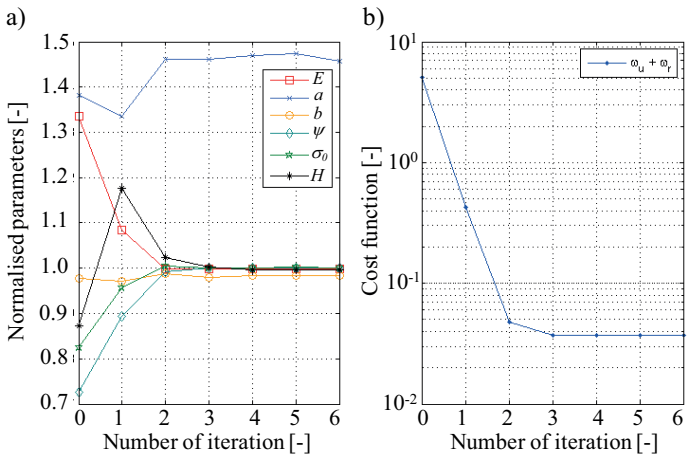

Figure 14: (a) Convergence curves for **exponential DP** constitutive law with hardening defined by **tension** yield stress σ_0, pseudo-experimental approach with noised data (accuracy - 1μm), (b) Convergence of cost function

REFERENCES

Bolzon, G. & V. Buljak (2011). An indentation-based technique to determine in-depth residual stress profiles induced by surface treatment of metal components. *Fatigue & Fracture of Engineering Materials & Structures 34*(2), 97–107.

Bolzon, G., V. Buljak, & E. Zappa (2012). Characterization of fracture properties of thin aluminum inclusions embedded in anisotropic laminate composites. *Frattura ed Integrita Strutturale 19*, 20–28.

Burczynski, T. & M. Szczepanik (2013). Intelligent optimal design of spatial structures. *Computers & Structures 127*, 102 – 115.

de Souza Neto, E., D. Peri, & D. Owen (2008). *Computational Methods for Plasticity: Theory and Applications*. Wiley.

Dlugosz, A. & T. Burczynski (2012). Multiobjective shape optimization of selected coupled problems by means of evolutionary algorithms. *Bulletin of the Polish Academy of Sciences. Technical Sciences Vol. 60, nr 2*, 215–222.

Drucker, D. C. & W. Prager (1952). Soil mechanics and plastic analysis or limit design. *Quarterly of Applied Mathematics 10*, 157–165.

Gajewski, T. & T. Garbowski (2014). Calibration of concrete parameters based on digital image correlation and inverse analysis. *Archives of Civil and Mechanical Engineering*. http://dx.doi.org/10.1016/j.acme.2013.05.012.

Garbowski, T., G. Maier, & G. Novati (2011). Diagnosis of concrete dams by flat-jack tests and inverse analyses based on proper orthogonal decomposition. *Journal of Mechanics of Materials and Structures 6*(1-4), 181–202.

Garbowski, T., G. Maier, & G. Novati (2012). On calibration of orthotropic elastic-plastic constitutive models for paper foils by biaxial tests and inverse analyses. *Structural and Multidisciplinary Optimization 46*(1), 111–128.

Lubliner, J., J. Oliver, S. Oller, & E. Oate (1989). A plastic-damage model for concrete. *International Journal of Solids and Structures 25*(3), 299–326.

Maier, G., G. Bolzon, V. Buljak, T. Garbowski, & B. Miller (2010). Synergistic combinations of computational methods and experiments for structural diagnosis. In M. Kuczma and K. Wilmanski (Eds.), *Computer Methods in Mechanics. Lectures of the CMM 2009*, pp. 453–476. Springer-Varlag Berlin Heidelberg.

Maier, G., V. Buljak, T. Garbowski, G. Cocchetti, & G. Novati (2014). Mechanical characterization of materials and diagnosis of structures by inverse analyses: some innovative procedures and applications. *International Journal of Comutational Methods*. DOI: 10.1142/S0219876213430020.

Nocedal, J. & S. Wright (2006). *Numerical Optimization*. Springer.

Pan, B., K. Qian, H. Xie, & A. Asundi (2009). Two-dimensional digital image correlation for in-plane displacement and strain measurement: A review. *Measurement Science and Technology 20*(6).

Rankine, W. J. M. (1857). On the stability of loose earth. *Philosophical Transactions of the Royal Society of London 147*, 9–27.

Resende, L. & J. B. Martin (1985). Formulation of drucker-prager cap model. *Journal of Engineering Mechanics 111*, 855–881.

Sutton, M. A., J. J. Orteu, & H. Schreier (2009). *Image Correlation for Shape, Motion and Deformation Measurements*. Springer.

Tekieli, M. & M. Slonski (2013). Computer vision based method for real time material and structure parameters estimation using digital image correlation, particle filtering and finite element method. In L. Rutkowski, M. Korytkowski, R. Scherer, R. Tadeusiewicz, L. Zadeh, and J. Zurada (Eds.), *Artificial Intelligence and Soft Computing*, Volume 7894 of *Lecture Notes in Computer Science*, pp. 624–633. Springer Berlin Heidelberg.

Wierzchon, S. T., J. J. Cochran, L. A. Cox, P. Keskinocak, J. P. Kharoufeh, & J. C. Smith (2010). *Simulated Annealing*. John Wiley & Sons, Inc.

Zirpoli, A., G. Novati, G. Maier, & T. Garbowski (2008). Dilatometric tests combined with computer simulations and parameter identification for in-depth diagnostic analysis of concrete dams. In F. Biondini and D. Frangopol (Eds.), *International Symposium on Life-Cycle Civil Engineering IALCCE '08*, pp. 259–264. CRC Press.